

# High-Performance Model Predictive Control for Quadcopters with Formal Stability Guarantees

Maedeh Izadi <sup>a</sup>, A.T.J.R. Cobbenhagen <sup>a</sup>, Ruben Sommer <sup>b</sup>, A.R.P. Andrien <sup>a</sup>,  
Erjen Lefeber <sup>a</sup>, W.P.M.H. (Maurice) Heemels <sup>a</sup>

<sup>a</sup>*Department of Mechanical Engineering, Eindhoven University of Technology, The Netherlands.*

<sup>b</sup>*Avular Mobile Robotics, Eindhoven, The Netherlands.*

---

## Abstract

In this paper, we present a novel cascade control structure with formal guarantees of uniform almost global asymptotic stability for the state tracking error dynamics of a quadcopter. The proposed approach features a model predictive control strategy for the outer loop, explicitly accounting for the non-zero total thrust constraint. The outer-loop controller generates an acceleration reference, which is then converted into attitude, angular velocity and acceleration references, subsequently tracked by a nonlinear inner-loop controller. The proposed cascade control strategy is validated through numerical case studies, underlying high-fidelity models, demonstrating its ability to track fast trajectories with small error.

*Key words:* Model predictive control, uniform global asymptotic stability, inner–outer loop control structure, quadcopter.

---

## 1 Introduction

Quadcopters have become a prominent category of UAVs with a broad range of practical applications, including infrastructure inspection [5], search-and-rescue missions [22], agriculture [23], wildlife monitoring [18], and medicine delivery [3]. This growing interest in quadcopters has driven the development of controllers capable of moving from laboratory demonstrations to real-world scenarios, calling for levels of high performance and robustness, while respecting the often limited on-board computational capabilities of quadcopters.

The control of quadcopters, especially trajectory tracking, is challenging due to the system’s open-loop instability, nonlinear dynamics, and underactuated configuration. The differential flatness property of quadcopters [10] can be employed for trajectory planning to achieve a user-specified goal. Various strategies are used to address the trajectory tracking problem for quadrotors, including sliding mode control [16], nonlinear PID control

[9], iterative learning control [11], nonlinear control [17], reinforcement learning [12], and model predictive control [10]. Among the numerous methods for quadcopter control, it is still rare to find a comprehensive control approach in the literature that offers four highly desired features: (i) anticipating future reference information, (ii) handling state and input constraints, (iii) real-time implementability on on-board embedded hardware, and (iv) stability guarantees. Research into quadcopter trajectory tracking control satisfying all these four features has mainly been pursued using Model Predictive Control (MPC) due to its ability to handle constraints, predictive behavior, and the availability of theoretical frameworks to provide stability guarantees (see [2]).

In [19], the differential flatness property of quadcopters is utilized to develop a real-time trajectory generation method. Conservative box constraints are then applied to create a convex feasible acceleration set using decoupled per-axis acceleration limits, followed by solving a convex optimization problem with bounds on each decoupled axis. In [4], a two-layer MPC approach is proposed, in which stabilization is managed by a linear constrained MPC controller, while at a higher hierarchical level and at a lower sampling rate, a hybrid MPC controller generates the online path for reaching a target position, considering obstacle avoidance. This real-time trajectory generation is especially advantageous in sce-

---

*Email addresses:* m.izadi.najafabadi1@tue.nl (Maedeh Izadi), a.t.j.r.cobbenhagen@tue.nl (A.T.J.R. Cobbenhagen), r.sommer@avular.com (Ruben Sommer), a.andrien@gmail.com (A.R.P. Andrien), a.a.j.lefeber@tue.nl (Erjen Lefeber), m.heemels@tue.nl (W.P.M.H. (Maurice) Heemels).

narios, where target and obstacle positions are unknown in advance, distinguishing it from offline planning methods. In [6], a feedback linearization model predictive control algorithm is developed for quadcopter trajectory tracking, aiming to achieve a more accurate linearized predictive model compared to Taylor series-based approximations. However, the last cited three papers do not include formal stability guarantees.

In addition to the linear MPC-based approach mentioned above, more recent papers have employed Nonlinear Model Predictive Control (NMPC) due to the enhanced onboard computational power of most quadcopters. In [13], an LQR controller with integral action is applied in the outer loop, while NMPC is used for attitude control in the inner loop. Despite introducing terminal constraints in the NMPC problem to stabilize the system, there is no global stability guarantee offered for the closed-loop system. In [8], a stability-guaranteed NMPC scheme is presented for quadcopters, determining the minimal stabilizing prediction horizon for asymptotic stability. This work proposes distinct running cost to achieve stability without relying on terminal conditions. Although of interest, a formal proof of stability is missing due to the forward Euler discretization of the nonlinear model instead of an exact method.

A cascade control approach, recently proposed in [2], combines linear MPC for outer-loop position control with nonlinear inner-loop attitude control. This method ensures uniform almost global asymptotic stability (UaGAS) while managing the quadcopter’s thrust constraint. However, its real-life performance falls short due to the conservatism introduced by translating nonlinear model constraints to linear ones and adding an auxiliary stabilizing constraint in the MPC. Hence, a quadcopter controller with the above-mentioned four features (i)–(iv) and additional high tracking performance is currently lacking.

Motivated by this gap in the literature, we propose a cascade control structure with a new MPC strategy in the outer loop, offering all four key features of an effective control approach, while also providing high-performance in the sense of being capable of tracking fast references with small error. In the outer loop, the translational system, including position and velocity dynamics, is modeled as a 12th-order linear problem. The MPC strategy is then applied to address the outer-loop problem. The non-zero total thrust constraint from the original nonlinear model is translated into constraints for the linear model. Our approach decouples both dynamics and constraints, resulting in three separate 4th-order linear MPC formulations for the  $x$ ,  $y$ , and  $z$  directions, each subject to time-varying (TV) decoupled linear constraints. This decoupling enhances real-time implementability and is thus important to warrant feature (iii) of a desirable controller. These three MPC controllers generate a twice-differentiable

virtual acceleration, which is then used to compute the thrust control input. The desired virtual acceleration is subsequently converted into a desired attitude, tracked in the inner loop by the nonlinear attitude controller from [17]. In [2], a stabilizing input constraint is added to ensure uniform global asymptotic stability (UGAS) of the MPC strategy, which introduces conservatism and results in reduced performance. Since the outer-loop dynamics are controllable and marginally stable<sup>1</sup>, we use a particular cost function proposed in [15] to ensure UGAS of the outer loop without compromising performance. Compared to [2], we propose a more efficient outer-loop MPC strategy for quadcopters by: (i) imposing less conservative constraints through time-varying constraints, rather than time-invariant ones, while still ensuring inter-sample constraint satisfaction; (ii) enhancing performance by employing an appropriate terminal cost instead of adding conservatism through auxiliary stabilizing constraints. These innovations require new technical developments and are instrumental for guaranteeing performance, as evidenced by high-fidelity numerical case studies.

The outline of this paper is as follows: Section 2 introduces the preliminaries and Section 3 presents the quadcopter dynamics model and the problem statement. Section 4 introduces the cascade configuration and defines the inner-loop and outer-loop problems. Section 5 details the inner-loop controllers, while Section 6 describes the structure of the outer loop. The MPC strategy in the outer loop is proposed in Section 7. The stability of the continuous-time system and cascade trajectory tracking are demonstrated in Sections 8 and 9, respectively. Section 10 presents numerical case studies, underlying high-fidelity models, and Section 11 concludes the work.

## 2 Preliminaries

This section introduces the notation, lemmas and theorems used throughout the paper. We utilize  $\mathbb{R}$ ,  $\mathbb{R}_{>0}$ , and  $\mathbb{R}_{\geq 0}$  to denote the set of real numbers, the set of positive real numbers, and the set of non-negative numbers, respectively. Additionally,  $\mathbb{R}^n$  represents the set of all  $n$ -dimensional vectors of real numbers. The set of natural numbers is denoted by  $\mathbb{N} = \{1, 2, 3, \dots\}$ , and  $\mathbb{N}_0 = \mathbb{N} \cup \{0\}$ . The symbol  $I$  is an identity matrix of appropriate dimensions. The 2-norm of a vector  $v \in \mathbb{R}^n$  is  $\|v\| = \sqrt{v^\top v}$ . A diagonal matrix with diagonal elements  $a_1, a_2, \dots, a_n$  is denoted as  $\text{diag}(a_1, a_2, \dots, a_n)$ .  $SO(3)$  is the group of 3-by-3 orthonormal matrices that represent rotations about the origin in  $\mathbb{R}^3$ . This work considers UGAS, and uniform local exponential stability (ULES), with their definitions provided in [14], and adopts UaGAS, which is UGAS except for a measure-zero set of initial conditions, as defined in [17]. The saturation function  $\text{sat} : \mathbb{R}^m \rightarrow \mathbb{R}^m$  is defined as  $\text{sat}(u) =$

<sup>1</sup> All eigenvalues lie within the unit circle and those on the unit circle are simple.

$[\text{sat}(u_1), \text{sat}(u_2), \dots, \text{sat}(u_m)]^\top$ , where

$$\text{sat}(u_i) = \begin{cases} u_{\max}, & u_i > u_{\max} \\ u_i, & |u_i| \leq u_{\max} \\ -u_{\max}, & u_i < -u_{\max} \end{cases} \quad (1)$$

for  $i \in \{1, 2, \dots, m\}$ , assuming  $u_{\max} > 0$  is clear from the context. Consider the discrete-time system

$$x^+ = Ax + B\text{sat}(u), \quad (2)$$

where  $x \in \mathbb{R}^n$  and  $u \in \mathbb{R}^m$  denote the current states and inputs, respectively. It is assumed that  $(A, B)$  is controllable, and the system is marginally stable. In this paper, the stability proof of the proposed MPC strategy is built on the theorems and lemmas from [15], which are repeated here for self-containment.

Marginal stability implies the existence of a positive definite matrix  $M_c$ , such that

$$A^\top M_c A - M_c \preceq 0. \quad (3)$$

A globally stabilizing small-gain control is defined as

$$u(x) = -\kappa B^\top M_c A x =: Kx, \quad (4)$$

where  $\kappa > 0$  is chosen such that

$$\kappa B^\top M_c B \prec I. \quad (5)$$

As demonstrated in [15], there exists a positive definite matrix  $M_q$  such that

$$(A + BK)^\top M_q (A + BK) - M_q = -I. \quad (6)$$

The following theorem outlines the stability properties of the resulting closed-loop system.

**Theorem 1** ([15]). *For the closed-loop system (2) with the small-gain control (4), assuming that  $(A, B)$  is controllable and (2) is marginally stable, there exist a global Lyapunov function  $W : \mathbb{R}^n \rightarrow \mathbb{R}_{>0}$  such that*

$$W(x) = W_q(x) + \lambda W_c(x) = x^\top M_q x + \lambda (x^\top M_c x)^{3/2} \quad (7)$$

$$W(Ax + B\text{sat}(Kx)) - W(x) \leq -\|x\|^2, \quad (8)$$

with  $K$  in (4),  $M_c \succ 0$  as in (3),  $M_q \succ 0$  specified in (6), and

$$\lambda = \frac{2\kappa L_u \sigma_{\max}(A_d^\top M_q B_d)}{\sqrt{\lambda_{\min}(M_c)}}, \quad (9)$$

where  $\sigma_{\max}$  and  $\lambda_{\min}$  denote the maximum singular value and minimum eigenvalue of a matrix, respectively and  $L_u$  is chosen such that  $L_u u_{\max} > 1$ .

On the basis of the Theorem 1 and using the following lemma, a globally stabilizing MPC for (2) can be derived.

**Lemma 1** ([15]). *Consider a discrete-time system described by  $x^+ = Ax + Bu$ , where  $x \in \mathbb{R}^n$ ,  $u \in \mathbb{R}^m$ ,  $(A, B)$  is controllable, and the optimal control sequence  $u^*(x) = (u_{0|k}^*(x), u_{1|k}^*(x), \dots, u_{N|k}^*(x))$  obtained from*

$$\begin{aligned} \min_u \quad & J_N(x, u) = V(x_{N|k}) + \sum_{i=0}^{N-1} l(x_{i|k}, u_{i|k}) \\ \text{s.t.} \quad & x_{0|k} = x, \\ & x_{i+1|k} = Ax_{i|k} + Bu_{i|k}, \quad i \in \{0, 1, \dots, N-1\}, \\ & u_{i|k} \in \mathcal{U}, \quad i \in \{0, 1, \dots, N-1\}, \end{aligned} \quad (10)$$

where

$$l(x_{i|k}, u_{i|k}) = x_{i|k}^\top Q x_{i|k} + u_{i|k}^\top R u_{i|k}, \quad (11)$$

with  $Q$  and  $R$  positive definite,  $V : \mathbb{R}^n \rightarrow \mathbb{R}_{>0}$  represents the terminal cost and is chosen such that  $V$  is a control Lyapunov function,  $\mathcal{U}$  represents the input constraint set, and  $J_N^*(x) = J_N(x, u^*)$  is the optimal cost. If there exist a local control law  $k_f : \mathbb{R}^n \rightarrow \mathbb{R}^m$  such that

- (1)  $k_f(x) \in \mathcal{U}$ ;
- (2)  $V(Ax + Bk_f(x)) - V(x) + l(x, k_f(x)) \leq 0$ ;
- (3)  $\alpha_1(\|x\|) \leq J_N^*(x) \leq \alpha_2(\|x\|)$ ,

with  $\alpha_1$  and  $\alpha_2$   $\mathcal{K}_\infty$ -functions<sup>2</sup>, then the MPC optimization problem is guaranteed feasible, guaranteeing  $x^+ = Ax + Bk_N(x)$  is globally asymptotically stable, and

$$J_N^*(x^+) = J_N^*(Ax + Bk_N(x)) \leq J_N^*(x) - l(x, k_N(x)),$$

with the MPC law

$$k_N(x) = u_{0|k}^*(x). \quad (12)$$

A globally stabilizing MPC strategy for the system (2) can now be derived, as outlined in Theorem 2.

**Theorem 2** ([15]). *Consider the closed-loop system (2), with the control law  $k_N(x)$  as in (12), resulting from the optimization problem*

$$\begin{aligned} \min_u \quad & J_N(x, u) = V(x_{N|k}) + \sum_{i=0}^{N-1} l(x_{i|k}, u_{i|k}) \\ \text{s.t.} \quad & x_{0|k} = x, \\ & x_{i+1|k} = Ax_{i|k} + Bu_{i|k}, \quad i \in \{0, 1, \dots, N-1\}, \\ & u_{i|k} \in [-u_{\max}, u_{\max}], \quad i \in \{0, 1, \dots, N-1\}, \end{aligned} \quad (13)$$

where  $V(x_{N|k}) = \Theta W(x_{N|k})$ ,  $W$  as in (7),  $l$  defined in (11),  $N \in \mathbb{N}$  is the prediction horizon,  $Q$  and  $R$  being positive definite and  $\Theta$  is a positive constant such that

$$\Theta \geq \lambda_{\max}(Q + \kappa^2 A^\top M_c B R B^\top M_c A). \quad (14)$$

<sup>2</sup> A function  $\alpha : [0, \infty) \rightarrow [0, \infty)$  is in class  $\mathcal{K}_\infty$  if it is strictly increasing,  $\alpha(0) = 0$ , and  $\alpha(r) \rightarrow \infty$  as  $r \rightarrow \infty$  ([15]).

Then, given any positive integer  $N$ , the closed-loop system  $x^+ = Ax + Bk_N(x)$  is globally asymptotic stable and

$$J_N^*(Ax + Bk_N(x)) - J_N^*(x) \leq -l(x, k_N(x)) \quad (15)$$

for all  $x \in \mathbb{R}^n$ .

**Remark 1** Given that for time-invariant finite-dimensional systems, global asymptotic stability is equivalent to UGAS, we can infer that the MPC control strategy outlined in Theorem 2 ensures UGAS.

Due to the cubic term in the terminal cost, the proposed MPC in Theorem 2 is not a QP problem, but it is convex and is solvable with convex optimization solvers.

### 3 Dynamics and Problem Setup

The model used in this work is based on the one presented in [2]. Let  $G$  be a right-handed inertial (or world) frame using the North-East-Down (NED) convention, with  $\{x_G, y_G, z_G\}$  as its orthonormal basis vectors.  $B$  represents a right-handed body-fixed frame with orthonormal basis vectors  $\{x_B, y_B, z_B\}$ , representing the axes of  $B$  relative to  $G$ . The rotation matrix  $R = [x_B, y_B, z_B] \in SO(3)$  defines the orientation of the body-fixed frame relative to the world frame. In addition, angular velocity, linear velocity and position of the body with respect to the world frame are described with vectors  $\omega = [\omega_1, \omega_2, \omega_3]^T$ ,  $v = [v_x, v_y, v_z]^T$  and  $p = [p_x, p_y, p_z]^T \in \mathbb{R}^3$ , respectively. With the defined variables, the dynamics of the quadcopter can be described as

$$\dot{p} = v, \quad (16a)$$

$$\dot{v} = gz_G - Tz_B - D^T v, \quad (16b)$$

$$\dot{R} = RS(\omega), \quad (16c)$$

$$J\dot{\omega} = S(J\omega)\omega - \tau_g - AR^T v - C\omega + \tau, \quad (16d)$$

where  $g$  is the gravitational acceleration,  $T \geq 0$  represents the magnitude of the combined thrust of the four propellers, normalized by mass,  $D = \text{diag}(d_x, d_y, d_z)$ ,  $d_x, d_y, d_z > 0$ , are the mass-normalized rotor drag coefficients,  $\tau_g \in \mathbb{R}^3$  are torques resulting from gyroscopic effects,  $J \in \mathbb{R}^{3 \times 3}$  is the inertia matrix,  $A$  and  $C$  are constant matrices,  $\tau = [\tau_1, \tau_2, \tau_3]^T \in \mathbb{R}^3$  is the torque input and  $S(\omega)$  represents a skew-symmetric matrix such that  $S(a)b = a \times b$  for any vectors  $a, b \in \mathbb{R}^3$ .

The thrust is non-negative and limited according to

$$0 \leq T(t) \leq T_{\max}, \quad \text{for all } t \in \mathbb{R}_{\geq 0}, \quad (17)$$

where  $T_{\max} > g$ . This physical restriction arises because the propellers can generate only a limited upward thrust and must counteract the gravitational force.

A reference trajectory  $(\bar{p}, \bar{v}, \bar{R}, \bar{\omega}, \bar{T}(t), \bar{\tau}) : \mathbb{R}_{\geq 0} \rightarrow \mathbb{R}^3 \times \mathbb{R}^3 \times SO(3) \times \mathbb{R}^3 \times \mathbb{R} \times \mathbb{R}^3$  is referred to be a feasible

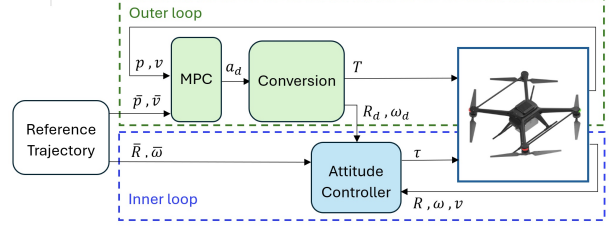


Fig. 1. Overview of the inner-outer loop control scheme: The outer loop MPC generates desired acceleration  $a_d$ , which is converted to thrust  $T$ , desired attitudes  $R_d$ , and angular velocities  $\omega_d$ , with  $T$  applied to the quadcopter. The inner-loop attitude controller uses  $R_d$ ,  $\omega_d$ , and measured attitudes and angular velocities to generate torque inputs  $\tau$  for the quadcopter.

trajectory, if it satisfies the dynamics (16) for all  $t \in \mathbb{R}_{\geq 0}$ , i.e.,

$$\dot{\tilde{p}} = \tilde{v}, \quad \dot{\tilde{v}} = gz_G - \bar{T}\bar{z}_B - D\tilde{v}, \quad (18a)$$

$$\dot{\tilde{R}} = \tilde{R}S(\tilde{\omega}), \quad J\dot{\tilde{\omega}} = S(J\tilde{\omega})\tilde{\omega} - \tau_g - A\tilde{R}^T\tilde{v} - C\tilde{\omega} + \tilde{\tau}, \quad (18b)$$

and  $0 < \epsilon_1 \leq \bar{T}(t) \leq T_{\max} - \epsilon_2$ , with fixed  $\epsilon_1, \epsilon_2 > 0$ .

For a feasible reference trajectory, the error coordinates are defined as

$$\tilde{p} = \bar{p} - p, \quad \tilde{v} = \bar{v} - v, \quad \tilde{R} = \bar{R}^T R, \quad \tilde{\omega} = \omega - \tilde{R}^T \bar{\omega}. \quad (19)$$

The main tracking control problem of the quadcopter can now be formulated as follows.

**Problem 1** ([2]). Given a feasible reference trajectory  $(\bar{p}, \bar{v}, \bar{R}, \bar{\omega}, \bar{T}, \bar{\tau})$ , develop appropriate control laws

$$T = T(p, v, R, \omega, \bar{p}, \bar{v}, \bar{R}, \bar{\omega}), \quad \tau = \tau(p, v, R, \omega, \bar{p}, \bar{v}, \bar{R}, \bar{\omega}),$$

such that (17) holds and the origin  $(\tilde{p}, \tilde{v}, \tilde{R}, \tilde{\omega}) = (0, 0, I, 0)$  of the resulting closed-loop system is UaGAS.

## 4 Controller Design

To address the tracking control problem outlined in Problem 1, a cascade control architecture is employed, consisting of an outer-loop and an inner-loop problem, that contain the translational (16a), (16b) and rotational (16c), (16d) dynamics, respectively, see Fig. 1. This section specifies the cascade configuration and introduces the problem definitions for the inner-loop and outer-loop problems.

### 4.1 Cascade trajectory tracking setup and constraints

The dynamics for position and velocity errors in (19) follow from (18a), (16a), and (16b), are given by

$$\dot{\tilde{p}} = \tilde{v}, \quad \dot{\tilde{v}} = -D\tilde{v} + Tz_B - \bar{T}\bar{z}_B.$$

A desired acceleration error  $a_d \in \mathbb{R}^3$  is defined as

$$a_d = Tz_B - \bar{T}\bar{z}_B. \quad (21)$$

So,  $T$  and  $z_B$  have to be chosen such that (21) holds. This allows the translational system, including the position and velocity dynamics, to be reformulated as a linear system

$$\dot{\tilde{p}} = \tilde{v}, \quad \dot{\tilde{v}} = -D\tilde{v} + a_d. \quad (22)$$

Thus, the first input  $T$  can be determined by

$$T = \|a_d + \bar{T}\bar{z}_B\|. \quad (23)$$

To track the desired virtual acceleration generated by the MPC in the outer loop, a desired thrust vector is generated and converted into a desired attitude. This attitude is then tracked using the torque  $\tau$  generated by the attitude tracking controller presented in Section 5. In [2], it is demonstrated how to achieve the desired attitude using the expression

$$R_d = [x_{B,d}, y_{B,d}, z_{B,d}], \quad (24)$$

where

$$\begin{aligned} z_{B,d} &= [z_{B,d_1} \ z_{B,d_2} \ z_{B,d_3}]^\top = \frac{\bar{R}^\top a_d + \bar{T}e_3}{\|\bar{R}^\top a_d + \bar{T}e_3\|}, \\ y_{B,d} &= \begin{bmatrix} 0 & \frac{z_{B,d_3}}{\sqrt{z_{B,d_2}^2 + z_{B,d_3}^2}} & \frac{-z_{B,d_2}}{\sqrt{z_{B,d_2}^2 + z_{B,d_3}^2}} \end{bmatrix}^\top, \\ x_{B,d} &= \begin{bmatrix} \sqrt{z_{B,d_2}^2 + z_{B,d_3}^2} & \frac{-z_{B,d_1}z_{B,d_2}}{\sqrt{z_{B,d_2}^2 + z_{B,d_3}^2}} & \frac{-z_{B,d_1}z_{B,d_3}}{\sqrt{z_{B,d_2}^2 + z_{B,d_3}^2}} \end{bmatrix}^\top. \end{aligned}$$

Subsequently, applying  $\dot{R}_d = R_d S(\omega_d)$  yields an expression for the desired angular velocity [2]

$$\omega_d = \begin{bmatrix} -y_{B,d}^\top \dot{z}_{B,d} & x_{B,d}^\top \dot{z}_{B,d} & -x_{B,d}^\top \dot{y}_{B,d} \end{bmatrix}^\top. \quad (25)$$

These derivations indicate that  $a_d$  can be tracked by determining the desired attitude in (24) and applying the thrust specified in (23). This means that when the errors (22) converge to zero,  $a_d$  also converges to zero and  $z_{B,d} \rightarrow e_3$ , causing  $R_d \rightarrow I$ . The inner-loop controller requires setpoints for the desired angular velocity and its derivative, so the desired acceleration must be twice differentiable.

The constraint (17) can be converted into a constraint on  $a_d$  by considering the following set of admissible values for the desired acceleration [2]:

$$\mathcal{A}(\bar{R}, \bar{T}) = \{a_d \in \mathbb{R}^3 \mid 0 < \|a_d + \bar{T}\bar{z}_B\| \leq T_{\max}, \bar{z}_B^\top a_d + \bar{T} > 0\}. \quad (26)$$

## 4.2 Cascade Problem Definition

To address Problem 1 using a cascade approach, we define two sub-problems: The outer-loop and inner-loop problems.

**Problem 2 (Outer-loop problem)** Find a virtual acceleration control law  $a_d = a_d(p, v, \bar{p}, \bar{v}, \bar{T})$ , which is twice differentiable with respect to time, such that the origin  $(\tilde{p}, \tilde{v}) = (0, 0)$  of the system (22) is UGAS and  $a_d(t) \in \mathcal{A}(\bar{R}, \bar{T})$  for all  $t \in \mathbb{R}_{\geq 0}$ , with  $\mathcal{A}(\bar{R}, \bar{T})$  as defined in (26).

Given the goal of steering  $\tilde{R}$  to  $R_d$  in the inner loop, attitude and angular velocity errors are formulated as

$$R_e = R_d^\top \tilde{R}, \quad (27a)$$

$$\omega_e = \omega - \tilde{R}^\top \bar{\omega} - R_e^\top \omega_d. \quad (27b)$$

The inner-loop problem is now defined as follows:

**Problem 3 (Inner-loop problem)** Find a control law  $\tau = \tau(R, \omega, \tilde{R}, \bar{\omega}, \bar{T}, a_d)$ , such that the origin  $(R_e, \omega_e) = (I, 0)$  of the system (27) is UaGAS.

## 5 Inner-loop Tracking

In this work, the non-linear controller from [17] is employed for stabilizing the attitude dynamics of the quadcopter, as it ensures ULES and UaGAS for the attitude dynamics. The input is given by

$$\begin{aligned} \tau &= -K_\omega \omega_e + K_R \sum_{i=1}^3 k_i (e_i \times R_e^\top e_i) \\ &\quad - S(J\omega)\omega + \tau_g + AR^\top v + C\omega \\ &\quad + J\tilde{R}^\top J^{-1}(S(J\bar{\omega})\bar{\omega} - \tau_g - A\bar{R}^\top \bar{v} - C\bar{\omega} + \bar{\tau}) \\ &\quad - J[(S(\omega)\tilde{R}^\top - \tilde{R}^\top S(\bar{\omega}))\bar{\omega} + S(\omega_e)R_e^\top \omega_d - R_e^\top \dot{\omega}_d], \end{aligned} \quad (28)$$

which results in the closed-loop system

$$\dot{R}_e = R_e S(\omega_e), \quad J\dot{\omega}_e = -K_\omega \omega_e + K_R \sum_{i=1}^3 k_i (e_i \times R_e^\top e_i),$$

for some  $k_i > 0$ ,  $K_\omega > 0$  and  $K_R > 0$ . Since  $R_e$  converges to  $I$  for almost all initial conditions, it can be concluded from (27a) that  $\tilde{R}$  converges to  $R_d$  for almost all initial conditions. Additionally, as  $\omega_e \rightarrow 0$ , (27b) implies that  $\bar{\omega} \rightarrow R_e^\top \omega_d$ . Combining this with  $R_e \rightarrow I$  results in  $\bar{\omega} \rightarrow \omega_d$ , thus solving Problem 3, see [2] for more details.

## 6 Outer-loop Dynamics and Constraints

As the MPC law employed in the outer loop will be formulated in discrete time, to ensure that the desired accelerations  $a_d$  remain twice differentiable, the translational error dynamics in (22) are extended to a 12th-order linear model [2]

$$\dot{\tilde{p}} = \tilde{v}, \quad (30a)$$

$$\dot{\tilde{v}} = -D\tilde{v} + a_d, \quad (30b)$$

$$\dot{a}_d = -\frac{1}{\gamma}(a_d - \eta), \quad (30c)$$

$$\dot{\eta} = -\frac{1}{\gamma}(\eta - s), \quad (30d)$$

with  $\gamma > 0$ ,  $\tilde{p}, \tilde{v}, a_d, \eta \in \mathbb{R}^3$  are the states and  $s \in \mathbb{R}^3$  is the input. Note that the dynamics in (30) are decoupled, allowing the dynamics in the  $x$ ,  $y$ , and  $z$  directions to be separated into three distinct fourth-order systems.

As detailed in Section 4.1,  $a_d$  must lie in the admissible set defined in (26). Given that  $\|a_d + \bar{T}\bar{z}_B\| \leq \|a_d\| + \bar{T}$ , when  $\|a_d\| + \bar{T} \leq T_{\max}$ , the condition  $\|a_d + \bar{T}\bar{z}_B\| \leq T_{\max}$  in (26) is satisfied, albeit with some conservatism. The second condition in (26), i.e.,  $\bar{z}_B^\top a_d + \bar{T} > 0$  is met, if  $\|a_d\| \leq \bar{T} - \delta$ , for some small  $0 < \delta < \epsilon_1$ . Therefore, a new and smaller set of admissible desired acceleration values,  $\mathcal{A}_o(\bar{T}) \subset \mathcal{A}(\bar{R}, \bar{T})$ , can be defined as

$$\mathcal{A}_o(\bar{T}) = \{a_d \in \mathbb{R}^3 \mid \|a_d\| \leq \rho(t)\}, \quad (31)$$

where

$$\rho(t) = \min(\bar{T}(t) - \delta, T_{\max} - \bar{T}(t)). \quad (32)$$

The approach in this work involves decoupling the non-linear constraint in (31). A box approximation is used, representing the largest cube that fits within the smaller sphere at each time instance. While this simplifies implementation, it introduces some level of conservatism. See Fig. 2. In this scenario,  $a_d$  is constrained to lie in a more conservative set,  $\mathcal{A}_c(\bar{T}) \subset \mathcal{A}_o(\bar{T}) \subset \mathcal{A}(\bar{R}, \bar{T})$ , such that

$$\mathcal{A}_c(\bar{R}, \bar{T}) = \{a_d \in \mathbb{R}^3 \mid |a_{d,i}(t)| \leq \Delta(t), i \in \{1, 2, 3\}\}, \quad (33)$$

where  $\Delta(t) = \frac{1}{\sqrt{3}}\rho(t)$ .

Decoupling the constraints simplifies control design and reduces online computational effort by solving three smaller 4th-order problems with decoupled linear constraints, but introduces conservatism due to the decoupled constraints. Note that in [2], the constraint is made time-invariant by considering the smallest sphere over all time, lower-bounding the TV bound in (33) by  $\Delta = \inf_{t \in \mathbb{R}_{\geq 0}} \Delta(t)$ , which introduces additional conservatism. To reduce conservatism in constraints compared to [2], we propose three separate linear MPC formulations, each subject to TV decoupled linear constraints instead of the time-invariant constraints. The TV nature of the constraints requires a significantly different MPC design compared to [2], as we will see in Section 7. In our approach,  $\mathcal{A}_o(\bar{T})$  is approximated by a TV cube with a side length of  $\frac{2\rho(t)}{\sqrt{3}}$ . See Fig. 2.

## 7 MPC Formulation

Upon decoupling the system (30), the dynamics of  $x$ ,  $y$ , and  $z$  are separated into three linear fourth-order mod-

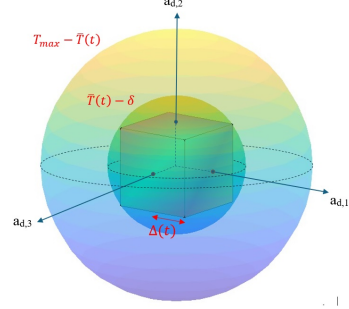


Fig. 2. Schematic of TV constraints on  $a_d$  in 3D. The radius of each sphere varies with the reference thrust  $\bar{T}$ , so the sphere with radius  $\bar{T}(t) - \delta$  is not always the smaller one. The cube illustrates the decoupled constraint, limiting each of the components of  $a_d$  to be within  $\pm\Delta(t)$ .

els:

$$\begin{aligned} \dot{\tilde{p}}^i &= \tilde{v}^i, & \dot{\tilde{v}}^i &= -d^i \tilde{v}^i + a_d^i, \\ \dot{a}_d^i &= -\frac{1}{\gamma}(a_d^i - \eta^i), & \dot{\eta}^i &= -\frac{1}{\gamma}(\eta^i - s^i), \end{aligned} \quad (34)$$

where  $i \in \{1, 2, 3\}$ ,  $\gamma > 0$ ,  $\tilde{p}^i, \tilde{v}^i, a_d^i, \eta^i \in \mathbb{R}$  are the states and  $s^i \in \mathbb{R}$  is the input. The system is subject to the TV constraint  $|a_{d,i}(t)| \leq \Delta(t)$ ,  $t \in \mathbb{R}_{\geq 0}$ , as in (33). The MPC law will be formulated in discrete time, thereby requiring the conversion of (34) to a discrete-time model. Using exact zero-order hold (ZOH) discretization, with  $s(t) = s(t_k)$ ,  $t \in [t_k, t_{k+1})$ ,  $t_k = kh$ ,  $k \in \mathbb{N}_0$ , and  $h > 0$  representing the sampling period, leads to the discrete-time system

$$x^+ = A_d x + B_d u, \quad (35)$$

where  $x = x(t_k)$ ,  $x = [\tilde{p} \ \tilde{v} \ a_d \ \eta]^\top \in \mathbb{R}^4$  representing the system states, and  $u = s(t_k) \in \mathbb{R}$  denotes the system input. The system matrices  $A_d$  and  $B_d$  are displayed in Table 1. Note that  $A_d$  has three eigenvalues inside the unit circle and one simple eigenvalue on the unit circle, indicating marginal stability of the system. The main continuous-time problem is subject to TV state constraints defined in (33). However, to obtain a discrete-time MPC setup, this constraint must be transformed into specific constraints on the sample times, while ensuring inter-sample constraints satisfaction. The following MPC problem is formulated for the outer loop:

$$\min_{U_k} J(x_k, U_k) = V(x_{N|k}) + \sum_{i=0}^{N-1} (x_{i|k}^\top Q x_{i|k} + u_{i|k}^\top R u_{i|k})$$

$$\text{s.t. } x_{0|k} = x_k,$$

$$x_{i+1|k} = A_d x_{i|k} + B_d u_{i|k}, \quad i \in \{0, 1, \dots, N-1\},$$

$$|u_{i|k}| \leq \Delta_{i|k}, \quad i \in \{0, 1, \dots, N-1\}, \quad (36a)$$

$$|a_{d,i|k}| \leq \Delta_{i|k}, \quad i \in \{0, 1, \dots, N\}, \quad (36b)$$

$$|\eta_{i|k}| \leq \Delta_{i|k}, \quad i \in \{0, 1, \dots, N\}, \quad (36c)$$

where

$$\Delta_{i|k} := \min_{t \in [t_{k+i}, t_{k+i+1})} \Delta(t), \quad (37)$$

with  $\Delta(t)$  defined in (33),  $U_k = [u_{0|k}, u_{1|k}, \dots, u_{N-1|k}]^\top$  contains the predicted future control inputs,  $N \in \mathbb{N}$  is

the prediction horizon,  $V : \mathbb{R}^4 \rightarrow \mathbb{R}_{\geq 0}$  represents the terminal cost and is chosen such that  $V$  is a control Lyapunov function,  $Q$  and  $R$  are positive definite,  $x_k$  is the state at discrete-time step  $k$ , and  $x_{i|k}$ ,  $u_{i|k}$  denote the prediction of the state and input at time step  $i+k$ , respectively, based on information available at time  $k$ .

The following sections address inter-sample constraint satisfaction, the conversion of state to input constraints, and the UGAS guarantee of the proposed MPC law.

### 7.1 Inter-sample constraints satisfaction

To achieve good tracking performance, especially in cases of long sampling periods, the MPC needs to account for the inter-sample behavior. The following lemma demonstrates that the MPC law in (36) ensures the satisfaction of constraint (33) between sample times.

**Lemma 2** *The MPC law resulting from the optimization problem (36) guarantees satisfaction of the constraint (33) between intersample intervals.*

**PROOF.** The evolution of the acceleration of the system (34) in between sample times equals

$$a_d(t) = \alpha(t-t_k) a_d(t_k) + \beta(t-t_k) \eta(t_k) + [1 - \alpha(t-t_k) - \beta(t-t_k)] u(t_k), \quad (38)$$

for  $t \in [t_k, t_{k+1})$ , where  $\alpha(t) = e^{-\frac{t}{\gamma}}$ ,  $\beta(t) = \frac{t}{\gamma} e^{-\frac{t}{\gamma}}$ . Note that  $0 < \alpha(t) \leq 1$ ,  $0 < \beta(t) \leq e^{-1}$ , and  $0 < \alpha(t) + \beta(t) \leq 1$ . In accordance with (38), at each time instance  $a_d(t)$  is a convex combination of  $a_d(t_k)$ ,  $\eta(t_k)$  and  $u(t_k)$ . Hence, from  $|a_d(t_k)| \leq \Delta_{0|k}$ ,  $|\eta(t_k)| \leq \Delta_{0|k}$  and  $|u(t_k)| \leq \Delta_{0|k}$ , we deduce that  $|a_d(t)| \leq \Delta_{0|k}$  for all  $t \in [t_k, t_{k+1})$ . Because  $\Delta_{0|k} \leq \Delta(t)$  for all  $t \in [t_k, t_{k+1})$  by definition, we can conclude that  $|a_d(t)| \leq \Delta(t)$  for all  $t$  within this interval.  $\square$

### 7.2 Converting the state constraints set into input constraints

The MPC problem (36) includes two state constraints and one input constraint. Terminal constraints are typically employed to guarantee stability and recursive feasibility in state-constrained linear receding horizon control schemes, but are often avoided due to their restrictive nature and complicating numerical optimization. In [20], a nonlinear mapping is derived that converts the state constraint set into an equivalent TV input constraint set for discrete-time linear systems. This approach anticipates the effect of current control actions on the future state and recalculates admissible control actions to prevent constraint violations. Using the subsequent two lemmas, the *state* constraints (36b) and (36c) are transformed into equivalent *input* constraints employing this method. The discrete-time dynamics of the states  $a_d$  and  $\eta$  of system (35) are formulated as follows:

$$a_d(k+1) = \alpha a_d(k) + \beta \eta(k) + [1 - \alpha - \beta] u(k), \quad (39)$$

$$\eta(k+1) = \alpha \eta(k) + [1 - \alpha] u(k), \quad (40)$$

where  $\alpha = e^{-\frac{h}{\gamma}}$ ,  $\beta = \frac{h}{\gamma} e^{-\frac{h}{\gamma}}$ , satisfying  $0 < \alpha \leq 1$ ,  $0 < \beta \leq e^{-1}$ , and  $0 < \alpha + \beta \leq 1$ .

**Lemma 3** *Consider the MPC problem defined in (36). If the TV input constraint*

$$\bar{\Delta}_{i|k}^- \leq u_{i|k} \leq \bar{\Delta}_{i|k}^+, \quad i \in \{0, 1, \dots, N-1\} \quad (41)$$

holds, where

$$\bar{\Delta}_{i|k}^+ := (1 - \alpha - \beta)^{-1} [\Delta_{i+1|k} - (\alpha a_{d_{i|k}} + \beta \eta_{i|k})], \quad (42)$$

$$\bar{\Delta}_{i|k}^- := (1 - \alpha - \beta)^{-1} [-\Delta_{i+1|k} - (\alpha a_{d_{i|k}} + \beta \eta_{i|k})], \quad (43)$$

then it also holds that  $|a_{d_{i+1|k}}| \leq \Delta_{i+1|k}$ .

**PROOF.** As mentioned,  $(1 - \alpha - \beta)$  is non-negative. Multiplying  $(1 - \alpha - \beta)$  to (41) and adding  $(\alpha a_{d_{i|k}} + \beta \eta_{i|k})$  to all three terms of the resulting inequalities yields

$$-\Delta_{i+1|k} \leq \alpha a_{d_{i|k}} + \beta \eta_{i|k} + (1 - \alpha - \beta) u_{i|k} \leq \Delta_{i+1|k}.$$

Using the dynamics of the state  $a_d$  in (39), it can be concluded that  $|a_{d_{i+1|k}}| \leq \Delta_{i+1|k}$ .  $\square$

**Lemma 4** *Consider the MPC problem defined in (36). If the TV input constraint*

$$\bar{\Delta}_{i|k}^- \leq u_{i|k} \leq \bar{\Delta}_{i|k}^+, \quad (44)$$

holds, where

$$\bar{\Delta}_{i|k}^+ := (1 - \alpha)^{-1} [\Delta_{i+1|k} - \alpha \eta_{i|k}], \quad (45)$$

$$\bar{\Delta}_{i|k}^- := -(1 - \alpha)^{-1} [\Delta_{i+1|k} + \alpha \eta_{i|k}], \quad (46)$$

then it implies that  $|\eta_{i+1|k}| \leq \Delta_{i+1|k}$ .

**PROOF.** Multiplying  $(1 - \alpha)$  to (44), adding  $\alpha a_{d_{i|k}}$ , and applying the same reasoning as in the proof of Lemma 3, yields  $|\eta_{i+1|k}| \leq \Delta_{i+1|k}$ .  $\square$

Leveraging Lemmas 3 and 4, the two state constraints (36b) and (36c) are replaced by their corresponding input constraints. As a result, all three constraints (36a)-(36c) can be unified into a single input constraint as

$$u_{i|k} \in [u_{\min_{i|k}}, u_{\max_{i|k}}], \quad i \in \{0, 1, \dots, N-1\}, \quad (47)$$

where

$$u_{\min_{i|k}} = \max(-\Delta_{i|k}, \bar{\Delta}_{i|k}^-, \bar{\Delta}_{i|k}^-), \quad (48)$$

$$u_{\max_{i|k}} = \min(+\Delta_{i|k}, \bar{\Delta}_{i|k}^+, \bar{\Delta}_{i|k}^+), \quad (49)$$

Table 1

State space matrices of the system in (35)

$$A_d = \begin{bmatrix} 1 & \frac{1-e^{-dh}}{d} & \frac{\gamma(e^{-dh}+d\gamma-d\gamma e^{-\frac{h}{\gamma}}-1)}{d(d\gamma-1)} & \frac{\gamma(e^{-dh}+2d\gamma-d^2\gamma^2-2d\gamma e^{-\frac{h}{\gamma}}-dhe^{-\frac{h}{\gamma}}+d^2\gamma^2 e^{-\frac{h}{\gamma}}+d^2\gamma he^{-\frac{h}{\gamma}}-1)}{d(d\gamma-1)^2} \\ 0 & e^{-dh} & \frac{\gamma(e^{-\frac{h}{\gamma}}-e^{-dh})}{d\gamma-1} & \frac{\gamma e^{-\frac{h}{\gamma}}+he^{-\frac{h}{\gamma}}-\gamma e^{-dh}-d\gamma he^{-\frac{h}{\gamma}}}{(d\gamma-1)^2} \\ 0 & 0 & e^{-\frac{h}{\gamma}} & \frac{h}{\gamma} e^{-\frac{h}{\gamma}} \\ 0 & 0 & 0 & e^{-\frac{h}{\gamma}} \end{bmatrix}$$

$$B_d = \begin{bmatrix} \frac{e^{-dh}+dh+3d^2\gamma^2-2d^3\gamma^3+d^3\gamma^2 h-3d^2\gamma^2 e^{-\frac{h}{\gamma}}+2d^3\gamma^3 e^{-\frac{h}{\gamma}}-2d^2\gamma h+d^3\gamma^2 he^{-\frac{h}{\gamma}}-d^2\gamma he^{-\frac{h}{\gamma}}-1}{d^2(d\gamma-1)^2} \\ \frac{1-e^{-dh}-2d\gamma+d^2\gamma^2+2d\gamma e^{-\frac{h}{\gamma}}+dhe^{-\frac{h}{\gamma}}-d^2\gamma^2 e^{-\frac{h}{\gamma}}-d^2\gamma he^{-\frac{h}{\gamma}}}{d(d\gamma-1)^2} \\ \frac{\gamma-\gamma e^{-\frac{h}{\gamma}}-he^{-\frac{h}{\gamma}}}{\gamma} \\ 1-e^{-\frac{h}{\gamma}} \end{bmatrix}$$

and  $\tilde{\Delta}_{i|k}^+$ ,  $\tilde{\Delta}_{i|k}^-$ ,  $\bar{\Delta}_{i|k}^+$  and  $\bar{\Delta}_{i|k}^-$  defined in (42), (43), (45) and (46). The necessary condition for the feasibility of the MPC problem with input constraint (47) is established in Theorem 3, ensuring that the input set is non-empty.

**Theorem 3** *If  $h$  and  $\gamma$  are appropriately chosen such that the condition*

$$\Delta(k+1) > e^{-\frac{h}{\gamma}} \left(1 + \frac{h}{\gamma}\right) \Delta(k), \quad \forall k \in \mathbb{N}_0, \quad (50)$$

*holds for a given finite-time trajectory with  $\Delta(k) = \Delta_{0|k}$  in (37), then the unified input constraint in (47) is non-empty, and the MPC controller (36) with the unified input constraint (47) will be feasible for all  $x \in \mathbb{R}^4$ .*

**PROOF.** See Appendix A.  $\square$

### 7.3 Stability Guarantee

This study aims to guarantee UGAS of the tracking error system for the proposed MPC strategy. In [2], a stabilizing input constraint is added to ensure the existence of a Lyapunov function, thus guaranteeing UGAS of the outer loop. However, adding a stabilizing input constraint compromises performance through the introduction of conservatism. Given that the system in (34) is marginally stable, an appropriate cost function can be used to find a Lyapunov function that guarantees the UGAS of the closed-loop system. As outlined in Section 2, a finite-horizon MPC is proposed in [15], which globally stabilizes marginally stable linear systems subject to input constraints by using a non-quadratic function as the terminal cost, consisting both cubic and quadratic functions of the state. This method is tailored to quadcopter setting here to ensure UGAS of the outer-loop problem without compromising performance. Since the MPC problem (36) deals with TV input constraints, it is necessary to derive conditions that ensure the validity of the proof of Theorem 2 for TV input constraints. Thus, a smaller time-invariant input set is derived in the following lemma, which is only used for the purpose of the

stability proof. This set serves as the saturation function (1), allowing Theorem 1 to be applied to determine the Lyapunov function.

**Lemma 5** *Consider the TV input set (47)*

$$\mathcal{U}_{i|k} = \{u \in \mathbb{R} \mid u_{\min_{i|k}} \leq u \leq u_{\max_{i|k}}\},$$

*with  $u_{\min_{i|k}}$  and  $u_{\max_{i|k}}$  defined in (48) and (49), then the following time-invariant input set is a subset of  $\mathcal{U}_{i|k}$  at all sample times  $k \in \mathbb{N}_0$ :*

$$\mathcal{U} = \{u \in \mathbb{R} \mid -\Delta^* \leq u \leq \Delta^*\}, \quad (51)$$

*where  $\Delta^*$  is a positive constant value obtained by*

$$\Delta^* = \min(\tilde{\Delta}_{\min}^+, \bar{\Delta}_{\min}^+, \Delta_{\min}), \quad (52)$$

*and*

$$\begin{aligned} \tilde{\Delta}_{\min}^+ &= (1 - \alpha - \beta)^{-1} \min_k [\Delta(k+1) - (\alpha + \beta)\Delta(k)], \\ \bar{\Delta}_{\min}^+ &= (1 - \alpha)^{-1} \min_k (\Delta(k+1) - \alpha\Delta(k)), \\ \Delta_{\min} &= \min_k \Delta(k), \end{aligned} \quad (53)$$

*with  $\Delta(k) = \Delta_{0|k}$  in (37).*

**PROOF.** See Appendix B  $\square$

Theorem 4 below presents the main contribution of this section, as it describes the design of an MPC problem with TV input constraints, ensuring UGAS and inter-sample constraint guarantees.

**Theorem 4** *Consider the closed-loop system (35), where the open-loop system is marginally stable and the pair  $(A_d, B_d)$  is controllable, with the control law  $k_N(x_k)$  as in (12), resulting from the optimization problem*

$$\min_{U_k} J(x_k, U_k) = V(x_{N|k}) + \sum_{i=0}^{N-1} (x_{i|k}^\top Q x_{i|k} + u_{i|k}^\top R u_{i|k})$$



$$\begin{aligned}
\text{s.t. } x_{0|k} &= x_k, & (54) \\
x_{i+1|k} &= A_d x_{i|k} + B_d u_{i|k}, \quad i \in \{0, 1, \dots, N-1\}, \\
u_{\min_{i|k}} &\leq u_{i|k} \leq u_{\max_{i|k}}, \quad i \in \{0, 1, \dots, N-1\},
\end{aligned}$$

where  $u_{\min_{i|k}}$  and  $u_{\max_{i|k}}$  defined in (48) and (49) and

$$V(x) = \Theta W(x) = \Theta \left[ x^\top M_q x + \lambda (x^\top M_c x)^{3/2} \right],$$

with  $M_c$  and  $M_q$  are as in (3) and (6),  $N \in \mathbb{N}$  is the prediction horizon,  $Q$  and  $R$  are positive definite matrices, and  $\Theta$  is as specified in (14). Furthermore, let  $h$  and  $\gamma$  be chosen appropriately such that

$$\Delta(k+1) > e^{-\frac{h}{\gamma}} \left( 1 + \frac{h}{\gamma} \right) \Delta(k), \quad \forall k \in \mathbb{N}_0,$$

for the given trajectory, with  $\Delta(k) = \Delta_{0|k}$  in (37). Then for any positive integer  $N$ , the closed-loop system  $x^+ = A_d x + B_d k_N(x)$  is uniformly globally asymptotically stable for

$$\lambda = \frac{2\kappa L_u \sigma_{\max}(A_d^\top M_q B_d)}{\sqrt{\lambda_{\min}(M_c)}},$$

where  $\kappa$  satisfies (5), and  $L_u$  is chosen such that  $\Delta^* L_u > 1$  with  $\Delta^*$  defined in (52) and (53).

**PROOF.** Consider the saturation function (1) with  $u_{\max} = \Delta^*$ . According to Theorem 1, the local control law  $k_f : \mathbb{R}^4 \rightarrow \mathbb{R}$ , defined as  $k_f(x) = \text{sat}(Kx)$  with the small gain control  $K$  in (4), ensures UGAS of the closed-loop system, with the global Lyapunov function defined in (7). Knowing that  $k_f(x) = \text{sat}(Kx)$ , we can infer that  $k_f(x) \in \mathcal{U}$  with  $\mathcal{U}$  defined in (51). By applying Lemma 5, it can be inferred that  $\mathcal{U} \subset \mathcal{U}_{i|k}$ . Demonstrating that  $k_f \in \mathcal{U}_{i|k}$ , the assumptions of Lemma 1 and Theorem 2 remains valid for a saturation function with  $u_{\max} = \Delta^*$ . Therefore, the MPC problem (54) demonstrates UGAS if  $L_u$  is chosen such that  $\Delta^* L_u > 1$ .  $\square$

## 8 Stability of the Continuous-time System

In Sections 7, UGAS is demonstrated for the proposed MPC strategy. The states in the discrete-time dynamics (35) exactly correspond to the states of the continuous-time dynamics (34) due to the exact discretization used. However, it is essential to take into account the behavior of the continuous-time system between sampling times to conclude UGAS for the continuous-time system. The continuous-time linear system (30) can be written as

$$\dot{x} = Ax(t) + Bu(t) \quad (55)$$

where  $x(t) = [\tilde{p}(t) \ \tilde{v}(t) \ a_d(t) \ \eta(t)]^\top \in \mathbb{R}^{12}$  and the input

$$u(t) = \begin{bmatrix} u_{x_{MPC}}(x(kh)) \\ u_{y_{MPC}}(x(kh)) \\ u_{z_{MPC}}(x(kh)) \end{bmatrix}, \quad \forall t \in [kh, kh+h), \quad (56)$$

is generated by three separate MPC problems. Then for all  $t \in [kh, kh+h)$ :

$$x(t) = e^{A(t-kh)} x(kh) + \int_{kh}^t e^{A(t-\tau)} d\tau B u(kh).$$

Knowing that matrix  $A$  represents the state matrix of a marginally stable system, we can infer that

$$\begin{aligned}
\|x(t)\| &= \|e^{A(t-kh)} x(kh) + \int_{kh}^t e^{A(t-\tau)} d\tau B u(kh)\| \\
&\leq \|e^{A(t-kh)}\| \|x(kh)\| + \left\| \int_{kh}^t e^{A(t-\tau)} d\tau B \right\| \|u(kh)\| \\
&\leq c_1 \|x(kh)\| + c_2 \|u(kh)\|.
\end{aligned}$$

In the formulated MPC strategy,  $u(kh)$  is constrained such that  $\|u(kh)\| \leq \Delta(t) = \frac{1}{\sqrt{3}} \rho(t)$  for all  $k \in \mathbb{N}_0$ , where

$$\rho(t) = \min(\bar{T}(t) - \delta, T_{\max} - \bar{T}(t)) \leq \max_t \bar{T}(t) \leq T_{\max}.$$

This bound on input, together with the UGAS property of  $x(kh)$  in discrete-time, ensures the states of the continuous-time system remain bounded between sampling times. Hence, the closed-loop system (55) with ZOH-input generated by MPC controllers, is guaranteed to be UGAS.

## 9 Cascade Trajectory Tracking Controller

The MPC controller in the outer-loop problem generates a desired acceleration, which has been demonstrated to be asymptotically stable. The desired acceleration is converted into a desired attitude, which is tracked by the attitude controller in the inner loop. The inner-loop controller has been proven to be ULES and UaGAS in [17]. To conclude the stability of the closed-loop system, it is necessary to demonstrate stability for the full cascade system. The closed-loop system resulting from the dynamics (16) and reference (18), with inputs defined in (23), (28), and (56), is expressed as:

$$\dot{\tilde{p}} = \tilde{v}, \quad (57a)$$

$$\dot{\tilde{v}} = -D\tilde{v} + a_d + TR(I - R_e^\top) e_3, \quad (57b)$$

$$\dot{a}_d = -\frac{1}{\gamma}(a_d + \eta), \quad (57c)$$

$$\dot{\eta} = -\frac{1}{\gamma}(\eta + u), \quad (57d)$$

$$\dot{R}_e = R_e S(\omega_e), \quad (57e)$$

$$J\dot{\omega}_e = -K_\omega \omega_e + K_R \sum_{i=1}^3 k_i (e_i \times R_e^\top e_i), \quad (57f)$$

which is a cascade of the systems (57a)-(57d) and (57e)-(57f).

**Theorem 5** *The origin  $(\tilde{p}, \tilde{v}, R_e, \omega_e) = (0, 0, I, 0)$  of (57) is UaGAS [2].*

**PROOF.** Given that the outer-loop dynamic (55) is UGAS on  $\mathbb{R}^{12}$  and the inner-loop dynamics is UaGAS on  $SO(3) \times \mathbb{R}^3$ , [2] demonstrates that if the solution remains bounded, UaGAS for (57) is guaranteed. The dynamics (57e)-(57f) are bounded since the inner-loop dynamics in (57) have been proven to be UaGAS on  $SO(3) \times \mathbb{R}^3$  in [17]. Therefore, demonstrating the boundedness of solutions for (57a)-(57d) suffices to ensure the stability of the full cascade system. For further details, refer to [2]. The boundedness of solutions for (57a)-(57d) is proved in Appendix C.  $\square$

Finally, it is demonstrated that achieving UaGAS for (57) provides a solution to Problem 1. Having UaGAS, as stated in Theorem 5, guarantees robustness against uniformly bounded perturbations, as described in [2].

**Corollary 1** *The controller, which uses the inputs derived from (23), (28), and (56), solves Problem 1.*

**PROOF.** See [2].

## 10 Numerical and High-Fidelity Case Studies

This section includes numerical case studies, using (16) as the quadcopter model, as well as high-fidelity case studies to verify the effectiveness of the proposed cascade control schemes. In particular, the dynamic in (35) is implemented for the state prediction process to obtain the solution of the MPC problem in the outer loop.

### 10.1 Numerical case study

In this section, we compare the proposed cascade control strategy with the controller from [2] through a numerical example. The simulations are conducted in MATLAB for a trajectory of 25 seconds. “*Proposed MPC*” refers to the MPC strategy formulated in Section 7, while the MPC strategy from [2] is labeled as “*Baseline MPC*” in the resulting plots. The nonlinear controller from Section 5 is employed for inner-loop control in both cases. Following [2], the dynamics in (16) for the simulation are based on the parameters used in [21]. These parameters are  $g = 9.81 \text{ m/s}^2$ ,  $J = \text{diag}(2.5, 2.1, 4.3) \text{ gm}^2$ ,  $D = \text{diag}(0.26, 0.28, 0.42) \text{ kg/s}$ ,  $\tau_g = [0, 0, 0]^T$ ,  $A = 0.1I$ ,  $C = 0.5I$ , and  $T_{\max} = 45.21 \text{ m/s}^2$ .

The challenging reference trajectory is considered as

$$\begin{aligned} \bar{p}(t) &= [2 \cos(4t) \quad 2 \sin(4t) \quad -10 + 2 \sin(2t)]^T, \\ \bar{\psi}(t) &= 0.2t, \end{aligned} \quad (58)$$

where  $\bar{p}(t)$  specifies the position reference and  $\bar{\psi}(t)$  represents the heading reference, indicating the angle between the projection of  $x_B$  onto the  $x_G - y_G$  plane and the  $x_G$  axis. This reference trajectory completely determines the states and inputs of the reference model in

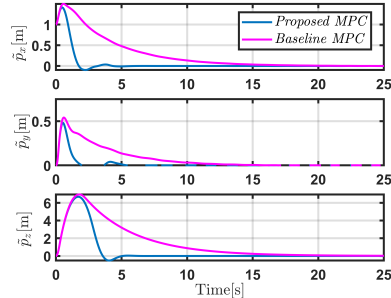


Fig. 3. Position errors  $\tilde{p} = [\tilde{p}_x, \tilde{p}_y, \tilde{p}_z]$  for each axes.

(18), based on the differential flatness property of the quadcopter [7].

The simulation starts from the same initial conditions as in the numerical example from [2]. The inner-loop gains are  $K_\omega = 30J$ ,  $K_R = 70J$ , and  $k = [4.5, 5, 5.5]$  in the simulation. The outer-loop parameters are  $h = 0.05 \text{ s}$ ,  $\gamma = 0.1$ ,  $N = 20$ ,  $Q = \text{diag}(100, 1, 1, 1)$ , and  $R = 0.01$ . To speed up the evaluation, CasADi [1] is used for solving the MPC problems, chosen for its efficiency in nonlinear optimization and compatibility with C++, Python, and MATLAB. The multiple shooting method is used in the MPC function code to improve convergence.

Fig. 3 shows that *Proposed MPC* outperforms *Baseline MPC*, highlighting its effectiveness in reducing conservatism and improving performance. The Root Mean Square Error (RMSE) for the *Proposed MPC* and *Baseline MPC* are  $[0.26, 0.07, 1.75] \text{ m}$  and  $[0.48, 0.14, 2.43] \text{ m}$ , respectively. The *Proposed MPC* executes in 3.3 ms on average, compared to 0.25 ms for the *Baseline MPC*. This increase in execution time is due to the fact that the *Proposed MPC* is not a QP problem. However, the execution time in both cases is significantly below the sampling period of  $h = 50 \text{ ms}$ . These results show that the *Proposed MPC* achieves a significantly lower RMSE compared to the *Baseline MPC*, but at the cost of increased computational time. Fig. 4 illustrates the desired acceleration in the  $x$ ,  $y$ , and  $z$  directions for both cases. It is evident that *Baseline MPC* applies more conservative constraints on  $a_d$ , showing that relaxing this constraint is instrumental in obtaining high performance. Both schemes satisfy UGAS property.

### 10.2 High-Fidelity Case Study

In this section we present numerical simulations in the Avular high-fidelity simulation environment for a quadcopter within MATLAB, aimed at validating the proposed cascade control strategy. The results are compared with a reference cascade control system that uses multiple PID controllers for altitude, horizontal position, and attitude control. Avular’s simulation environment incorporates the dynamics specified in (16) and also includes motor dynamics, sensor measurements, and state estimation to closely mimic real-world conditions. The

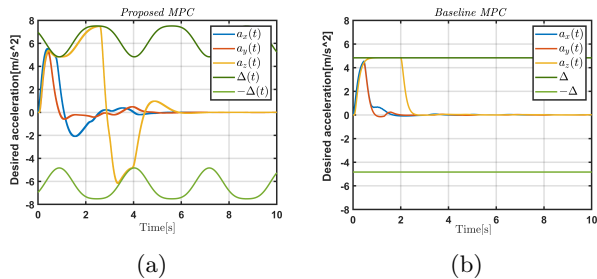


Fig. 4. Desired accelerations in  $x$ ,  $y$ , and  $z$  during the first 10 seconds of the simulations. (a) shows that the *Proposed MPC* keeps  $a_{d,i}$  within  $-\Delta(t)$  to  $\Delta(t)$ , satisfying constraint (33). (b) shows the *Baseline MPC*, where  $a_{d,i}$  are constrained within  $-\Delta$  to  $\Delta$ , reflecting its conservative nature.

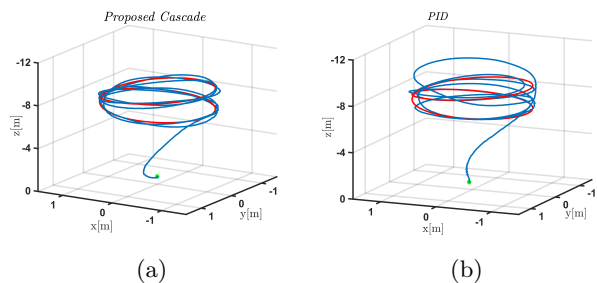


Fig. 5. 3D plot of the reference and actual trajectories, using the Avular high-fidelity simulation environment. The reference trajectory is indicated in red across both cases.

addition of artificial noise in sensor measurements and the subsequent state estimation introduces extra uncertainty. “*Proposed cascade*” refers to the control strategies formulated in Sections 5 and 7, whereas the cascade PID-based controller is labeled as “*PID*” in the resulting plots.

The Avular Vertex One parameters, utilized in the simulations are  $g = 9.81 \text{ m/s}^2$ ,  $J = \text{diag}(0.08, 0.08, 0.3) \text{ kgm}^2$ ,  $D = \text{diag}(0.15, 0.15, 0.15) \text{ kg/s}$ ,  $\tau_g = [0, 0, 0]^T$ ,  $A = 0.1I$ ,  $C = 0.5I$ ,  $T_{\max} = 80 \text{ N}$  and,  $m = 2.8 \text{ kg}$ . The inner-loop parameters are set to the same values as those in Section 10.1. The outer-loop parameters are  $h = 0.1 \text{ s}$ ,  $\gamma = 0.1$ ,  $N = 20$ ,  $Q = \text{diag}(100, 1, 1, 1)$ , and  $R = 1$ . The simulations are conducted for 30 seconds and the reference trajectory is considered as

$$\begin{aligned} \bar{p}(t) &= [\cos(0.4\pi t) \quad \sin(0.4\pi t) \quad -8 + \sin(0.2\pi t)]^T, \\ \bar{\psi}(t) &= 0.2t, \end{aligned} \quad (59)$$

Fig. 5 illustrates the reference and resulting position trajectories. As demonstrated by the trajectory plots and further validated by the position errors in Fig 6, *Proposed cascade* outperforms *PID*, highlighting its ability to effectively reduce overshoot in the  $z$ -direction step response, thanks to the predictive capability of MPC in anticipating future system behavior.

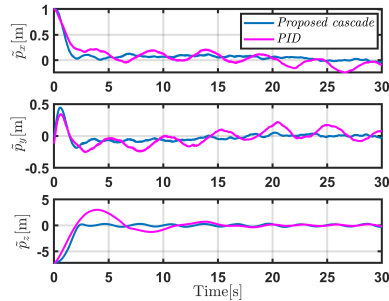


Fig. 6. Position errors  $\tilde{p} = [\tilde{p}_x, \tilde{p}_y, \tilde{p}_z]$  for each axes, using the Avular high-fidelity simulation environment.

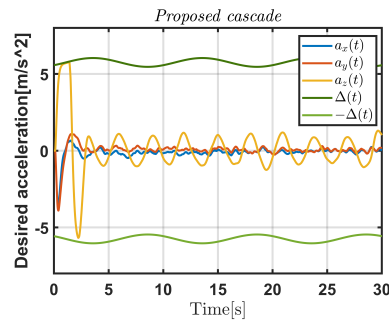


Fig. 7. Desired accelerations in the  $x$ ,  $y$ , and  $z$  directions for the *Proposed Cascade* in the Avular high-fidelity simulation environment show that the MPC controller keeps  $a_{d,i}$  within  $\pm\Delta(t)$ , satisfying constraint (33).

The Root Mean Square Error (RMSE) for the *Proposed cascade* and *PID* are  $[0.17, 0.086, 1.41]m$  and  $[0.20, 0.12, 1.47]m$ , respectively, demonstrating the effectiveness of the *Proposed cascade* in tracking fast trajectories with small error. Note that the *proposed cascade* not only outperforms *PID* with a lower RMSE but also offers formal stability guarantees, whereas *PID* does not provide such guarantees. Fig. 7 shows the desired accelerations in the  $x$ ,  $y$ , and  $z$  directions for *Proposed cascade*, highlighting that the desired acceleration constraints in (33) are met.

## 11 Conclusion

This paper has provided a cascade inner-outer loop control structure for trajectory tracking of a quadcopter, including a formal closed-loop tracking guarantee. The proposed approach has been based on a new MPC-based controller design for the outer loop, accounting for the quadcopter’s limited thrust capabilities and leading to high performance through a significantly less conservative design compared to earlier MPC proposals with stability guarantees. The combination of a UaGAS nonlinear controller in the inner loop and a UGAS MPC-based controller in the outer loop has enabled us to demonstrate UaGAS for the trajectory tracking errors of the entire cascade system.

To validate the proposed control schemes, we have con-

ducted a numerical case study to compare the performance of the proposed strategy with the controller from [2]. This comparison has highlighted how the proposed method improves the performance of the cascade control strategy, particularly by reducing conservatism. We have also validated the proposed cascade control strategy by comparing it with a reference PID-based cascade control system in the Avular high-fidelity simulation environment within MATLAB, using Avular Vertex One parameters. The results have shown that our proposed strategy outperforms PID-based cascade control system in navigating fast trajectories.

Future work will include relaxing the constraints on  $a_d$  by using the first original constraint from (26) and reducing the conservatism introduced by using the alternative constraint in (31). Particularly, the real-time feasibility of a novel MPC design with a coupled 12th-order model and coupled constraints, running on the quadcopter's on-board hardware platform, should be considered. Another avenue for future research involves conducting real-life experiments to validate the entire cascade scheme.

### A Appendix A. Proof of Theorem 3

If  $u_{min_{i|k}} \leq u_{i|k} \leq u_{max_{i|k}}$ , then

$$\tilde{\Delta}_{i|k}^- \leq u_{i|k} \leq \tilde{\Delta}_{i|k}^+, \quad (\text{A.1a})$$

$$\bar{\Delta}_{i|k}^- \leq u_{i|k} \leq \bar{\Delta}_{i|k}^+, \quad (\text{A.1b})$$

$$-\Delta_{i|k} \leq u_{i|k} \leq \Delta_{i|k}. \quad (\text{A.1c})$$

By meeting (A.1a) and (A.1b), in line with Lemma 3 and Lemma 4, we can ensure that  $|a_{d_{i+1|k}}| \leq \Delta_{i+1|k}$  and  $|\eta_{i+1|k}| \leq \Delta_{i+1|k}$  for  $i \in \{0, 1, \dots, N-1\}$ . So, by initializing the controller with  $|a_{d_{0|0}}| \leq \Delta_{0|0}$  and  $|\eta_{0|0}| \leq \Delta_{0|0}$ , we have  $|a_{d_{i|k}}| \leq \Delta_{i|k}$  and  $|\eta_{i|k}| \leq \Delta_{i|k}$  for all  $i \in \{0, 1, \dots, N\}$ .

If the lower bounds of these three input constraints (A.1a-A.1c) are negative and their upper bounds are positive, we ensure that the intersection of these three input constraint sets is not empty. Hence, to establish a single TV input constraint with a negative lower bound  $u_{min_{i|k}}$  and a positive upper bound  $u_{max_{i|k}}$ ,  $\tilde{\Delta}_{i|k}^-$  and  $\bar{\Delta}_{i|k}^-$  should be negative, while  $\tilde{\Delta}_{i|k}^+$  and  $\bar{\Delta}_{i|k}^+$  should be positive (knowing that  $\Delta_{i|k}$  is always positive). Considering  $|a_{d_{i|k}}| \leq \Delta_{i|k}$  and  $|\eta_{i|k}| \leq \Delta_{i|k}$ , it follows that

$$|\alpha a_{d_{i|k}} + \beta \eta_{i|k}| \leq (\alpha + \beta) \Delta_{i|k}, \quad |\alpha \eta_{i|k}| \leq \alpha \Delta_{i|k}. \quad (\text{A.2})$$

If  $h$  and  $\gamma$  are chosen such that  $\Delta_{i+1|k} > (\alpha + \beta) \Delta_{i|k}$  for all  $k \in \mathbb{N}_0$ , then we can infer from (A.2) that  $|\alpha a_{d_{i|k}} + \beta \eta_{i|k}| < \Delta_{i+1|k}$  and  $|\alpha \eta_{i|k}| < \Delta_{i+1|k}$ . Using (42), (43),

(45) and (46), it is evident that  $\tilde{\Delta}_{i|k}^-$  and  $\bar{\Delta}_{i|k}^-$  are negative, and  $\tilde{\Delta}_{i|k}^+$  and  $\bar{\Delta}_{i|k}^+$  are positive. Therefore, the input set in (47) is non-empty.

### B Appendix B. Proof of Lemma 5

To prove that  $\mathcal{U} \subset \mathcal{U}_{i|k}$ , it suffices to show that  $-\Delta^* \geq u_{min_{i|k}}$  and  $\Delta^* \leq u_{max_{i|k}}$  at all sample times  $k$ . According to (48) and (49), we have

$$\begin{aligned} \max_k(u_{min_{i|k}}) &= \\ & \max \left( \max_k -\Delta(k), \max_k \tilde{\Delta}^-(k), \max_k \bar{\Delta}^-(k) \right), \\ \min_k(u_{max_{i|k}}) &= \\ & \min \left( \min_k \Delta(k), \min_k \tilde{\Delta}^+(k), \min_k \bar{\Delta}^+(k) \right). \end{aligned}$$

Based on (42)

$$\tilde{\Delta}_{i|k}^+(k) = (1 - \alpha - \beta)^{-1} [ \Delta_{i+1|k} - (\alpha a_{d_{i|k}} + \beta \eta_{i|k}) ].$$

Given  $\alpha a_{d_{i|k}} + \beta \eta_{i|k} \leq (\alpha + \beta) \Delta_{i|k}$  from (A.2), we get

$$\tilde{\Delta}_{i|k}^+(k) \geq (1 - \alpha - \beta)^{-1} [ \Delta_{i+1|k} - (\alpha + \beta) \Delta_{i|k} ].$$

Minimizing both sides of the inequality over  $k$  leads to

$$\begin{aligned} \min_k \tilde{\Delta}^+(k) &\geq \\ & \underbrace{(1 - \alpha - \beta)^{-1} \min_k [\Delta(k+1) - (\alpha + \beta) \Delta(k)]}_{\tilde{\Delta}_{min}^+}. \end{aligned}$$

Similarly, using (43), (45), and (46), and considering (A.2), it can be concluded that

$$\begin{aligned} \min_k \bar{\Delta}^+(k) &\geq \underbrace{(1 - \alpha)^{-1} \min_k [\Delta(k+1) - \alpha \Delta(k)]}_{\bar{\Delta}_{min}^+}, \\ \max_k \tilde{\Delta}^-(k) &\leq \\ & \underbrace{-(1 - \alpha - \beta)^{-1} \min_k [\Delta(k+1) - (\alpha + \beta) \Delta(k)]}_{-\tilde{\Delta}_{min}^+}, \\ \max_k \bar{\Delta}^-(k) &\leq \underbrace{-(1 - \alpha)^{-1} \min_k [\Delta(k+1) - \alpha \Delta(k)]}_{-\bar{\Delta}_{min}^+}. \end{aligned}$$

So we have

$$\begin{aligned} \min_k(u_{max_{i|k}}) &\geq \min(\tilde{\Delta}_{min}^+, \bar{\Delta}_{min}^+, \Delta_{min}) = \Delta^*, \\ \max_k(u_{min_{i|k}}) &\leq \max(\underbrace{-\tilde{\Delta}_{min}^+, -\bar{\Delta}_{min}^+, -\Delta_{min}}_{-\Delta^*}), \end{aligned}$$

which implies  $\mathcal{U} \subset \mathcal{U}_{i|k}$  at all sample times  $k$ .

### C Appendix C. Proof of the boundedness of the solution for (57a)-(57d)

Using (55), the dynamics of (57a)-(57d) can be written as:

$$\dot{x}(t) = Ax(t) + Bu_{MPC}(x(kh)) + \begin{bmatrix} 0 \\ I_3 \\ 0 \\ 0 \end{bmatrix} TR(I - R_e^\top) e_3,$$

for all  $t \in [kh, kh+h)$  with  $x(t) \in \mathbb{R}^{12}$ . Inner-loop closed-loop system has  $(R_e(t), \omega_e(t)) = (I, 0)$  as a uniformly locally exponentially stable (ULES) and UaGAS equilibrium [17]. Given that  $x, y$  and  $z$  dynamics can be decoupled and  $T$  is globally bounded, only boundedness and stability of the following dynamics needs to be studied:

$$\dot{x}(t) = A'x(t) + B'u_{MPC}(x(kh)) + \begin{bmatrix} 0 \\ 1 \\ 0 \\ 0 \end{bmatrix} \phi(t), \quad (C.1)$$

for  $t \in [kh, kh+h)$  with  $x(t) \in \mathbb{R}^4$ ,  $A'$  and  $B'$  represent the system matrices of continuous-time dynamics (34) for a single axis. Since  $R(I - R_e^\top) e_3$  is ULES, there exist positive constants  $\lambda > 0$  and  $c' > 0$ , where  $c'$  depends on the initial condition  $(R_e(t_0), \omega_e(t_0))$ , such that  $|\phi(t)| \leq c'e^{-\lambda t}$ .

First step is to show boundedness of states at sample times. The discrete-time dynamics of the cascade system derived from (C.1) can be expressed as follows:

$$x(kh+h) = A_d x(kh) + B_d u_{mpc}(x(kh)) + \int_0^h e^{A's} \phi(kh+h-s) ds \begin{bmatrix} 0 \\ 1 \\ 0 \\ 0 \end{bmatrix},$$

with  $A_d$  and  $B_d$  defined in (35). Knowing that  $\left\| \int_0^h e^{A's} \phi(kh+h-s) ds \right\| \leq c'e^{-\lambda kh}$ , the discrete-time dynamics can be expressed as

$$x_{k+1} = f(x_k) + g(x_k, z_k)z_k, \quad (C.2)$$

where  $f(x_k) = A_d x_k + B_d u_{mpc}(x_k)$ ,  $g(x_k, z_k)$  is bounded and  $z_k$  is ULES and UaGAS, satisfying  $\|z_k\| \leq ce^{-\lambda kh}$ . As demonstrated in previous sections, the Lyapunov function for the outer-loop problem with dynamics

$$x_{k+1} = A_d x_k + B_d u_{mpc}(x_k) \text{ is}$$

$$V(x) = x^\top M_q x + \lambda (x^\top M_c x)^{\frac{3}{2}},$$

with  $M_q$  and  $M_c$  are positive definite matrices defined in (7). The Lyapunov function  $V(x_k)$  satisfies the following properties:

- (i)  $V(f(x_k)) - V(x_k) \leq 0$ , which implies  $\|f(x_k)\| \leq \|x_k\|$ ,
- (ii) there exists a positive constant  $l$  such that  $V(x_k) > l\|x_k\|^2$ ,

To establish the boundedness of the solution  $x_k$  of (C.2), it suffices to demonstrate the boundedness of the Lyapunov function. Leveraging the properties (i) and (ii) of the  $V(x)$ , the following inequality is derived for the dynamics formulated in (C.2):

$$\begin{aligned} V(x_{k+1}) - V(x_k) &= (f_k + g_k z_k)^\top M_q (f_k + g_k z_k) \\ &\quad + \lambda ((f_k + g_k z_k)^\top M_c (f_k + g_k z_k))^{\frac{3}{2}} - V(x_k) \\ &\leq 0 + c_1 \|x_k\| \|z_k\| + c_2 \|z_k\|^2 + c_3 \|x_k\|^{\frac{3}{2}} \|z_k\|^{\frac{3}{2}} \\ &\quad + c_4 \|z_k\|^3. \end{aligned}$$

Using the property (ii) of the  $V(x)$  and knowing that  $\|z_k\| \leq ce^{-\lambda kh}$ , it is deduced

$$\begin{aligned} V(x_{k+1}) &\leq V(x_k) + c_5 \sqrt{V(x_k)} e^{-\lambda_1 kh} \\ &\quad + c_6 V(x_k) e^{-\lambda_2 kh} + c_7 e^{-\lambda_3 kh}, \end{aligned}$$

where  $c_1, c_2, \dots, c_7 > 0$  and  $\lambda_1, \lambda_2, \lambda_3 > 0$ . Then  $V(x_{k+1})$  can be over-approximated as

$$\begin{aligned} V(x_{k+1}) &< (1 + c_8 e^{-\lambda_4 kh}) V(x_k) \\ &\quad + 2c_8 e^{-\lambda_4 kh} \sqrt{1 + c_8 e^{-\lambda_4 kh}} \sqrt{V(x_k)} + c_8^2 e^{-2\lambda_4 kh} \\ &= \left( \sqrt{1 + c_8 e^{-\lambda_4 kh}} \sqrt{V(x_k)} + c_8 e^{-\lambda_4 kh} \right)^2, \end{aligned}$$

where  $c_8 = \max(c_5, c_6, \sqrt{c_7})$  and  $\lambda_4 = \min(\lambda_1, \lambda_2, \frac{\lambda_3}{2})$ . Therefore, to demonstrate the boundedness of  $V(x_k)$ , it suffices to prove that the solution to the following difference equation remains bounded:

$$F_{k+1} = (a_k \sqrt{F_k} + b_k)^2,$$

where  $a_k = \sqrt{1 + c_8 e^{-\lambda_4 kh}}$  and  $b_k = c_8 e^{-\lambda_4 kh}$ . Considering  $F_k = G_k^2$  and given that  $a_k, b_k > 0$ , it is described by the linear difference equation  $G_{k+1} = a_k G_k + b_k$ , which can be solved iteratively as:

$$G_k = A_k G_0 + B_k, \quad G(0) = G_0,$$

with  $A_k = \prod_{i=0}^{k-1} a_i$ ,  $B_k = \sum_{j=0}^{k-1} (b_j \prod_{i=j+1}^{k-1} a_i)$ . To demonstrate the boundedness of the solution to the difference equation, it is necessary to prove that  $A_k$  and  $B_k$

remain bounded. Taking the logarithm of  $A_k$ :

$$\begin{aligned}\log(A_k) &= \log\left(\prod_{i=0}^{k-1} \sqrt{1 + c_8 e^{-\lambda_4 i h}}\right) \\ &= \frac{1}{2} \sum_{i=0}^{k-1} \log(1 + c_8 e^{-\lambda_4 i h}) \\ &\leq \frac{1}{2} \sum_{i=0}^{k-1} c_8 e^{-\lambda_4 i h} = \frac{c_8(1 - e^{-\lambda_4 k h})}{2(1 - e^{-\lambda_4 h})} \\ &\leq \frac{c_8}{2(1 - e^{-\lambda_4 h})},\end{aligned}$$

results in  $A_k \leq e^{\frac{c_8}{2(1 - e^{-\lambda_4 h})}}$ , which shows the boundedness of  $A_k$ . In addition,

$$\begin{aligned}B_k &= \sum_{j=0}^{k-1} \left( c_8 e^{-\lambda_4 j h} \prod_{i=j+1}^{k-1} \sqrt{1 + c_8 e^{-\lambda_4 i h}} \right) \\ &\leq \prod_{i=0}^{k-1} \sqrt{1 + c_8 e^{-\lambda_4 i h}} \sum_{j=0}^{k-1} c_8 e^{-\lambda_4 j h} \\ &= A_k \frac{c_8(1 - e^{-\lambda_4 k h})}{1 - e^{-\lambda_4 h}} \leq \frac{c_8}{1 - e^{-\lambda_4 h}} A_k.\end{aligned}$$

Thus  $G_k \leq \left(G_0 + \frac{c_8}{1 - e^{-\lambda_4 h}}\right) e^{\frac{c_8}{2(1 - e^{-\lambda_4 h})}}$ , which demonstrates the boundedness of  $G_k$ . Consequently, this implies the boundedness of  $F_k$  and  $V(x_k)$ , proving that the solution  $x_k = [\tilde{p}_k \ \tilde{v}_k \ a_{d_k} \ \eta_k]^\top$  of (C.2) remains bounded at each sample time. Moreover, continuity ensures boundedness in between sample times in this scenario.

## References

- [1] J. A. E. Andersson, J. Gillis, G. Horn, J. B. Rawlings, and M. Diehl. Casadi: A software framework for nonlinear optimization and optimal control. *Mathematical Programming Computation*, 11:1–36, 2019.
- [2] A. R. P. Andri n, E. Lefeber, D. Antunes, and W. P. M. H. Heemels. Model predictive control for quadcopters with almost global trajectory tracking guarantees. *IEEE Transactions on Automatic Control*, pages 5216–5230, 2024.
- [3] M. Balasingam. Drones in medicine—the rise of the machines. *International journal of clinical practice*, 71(9):e12989, 2017.
- [4] A. Bemporad, C. A. Pascucci, and C. Rocchi. Hierarchical and hybrid model predictive control of quadcopter air vehicles. *IFAC Proceedings Volumes*, 42(17):14–19, 2009.
- [5] A. Bircher, M. Kamel, K. Alexis, H. Oleynikova, and R. Siegwart. Receding horizon path planning for 3D exploration and surface inspection. *Autonomous Robots*, pages 291–306, 2018.
- [6] Z. Cai, S. Zhang, and X. Jing. Model predictive controller for quadcopter trajectory tracking based on feedback linearization. *IEEE Access*, 9:162909–162918, 2021.
- [7] M. Faessler, A. Franchi, and D. Scaramuzza. Differential flatness of quadrotor dynamics subject to rotor drag for accurate tracking of high-speed trajectories. *IEEE Robotics and Automation Letters*, 3(2):620–626, 2017.
- [8] M. A. Goma , O. De Silva, G. K. Mann, and R. G. Gosine. Computationally efficient stability-based nonlinear model predictive control design for quadrotor aerial vehicles. *IEEE Transactions on Control Systems Technology*, pages 615–630, 2022.
- [9] F. Goodarzi, D. Lee, and T. Lee. Geometric nonlinear pid control of a quadrotor uav on SE(3). In *IEEE European control conference (ECC)*, pages 3845–3850, 2013.
- [10] M. Greeff and A. P. Schoellig. Flatness-based model predictive control for quadrotor trajectory tracking. In *IEEE/RSJ International Conference on Intelligent Robots and Systems (IROS)*, pages 6740–6745, 2018.
- [11] M. Hehn and R. D’Andrea. A frequency domain iterative learning algorithm for high-performance, periodic quadcopter maneuvers. *Mechatronics*, pages 954–965, 2014.
- [12] J. Hwangbo, I. Sa, R. Siegwart, and M. Hutter. Control of a quadrotor with reinforcement learning. *IEEE Robotics and Automation Letters*, pages 2096–2103, 2017.
- [13] M. Kamel, K. Alexis, M. Achtelik, and R. Siegwart. Fast nonlinear model predictive control for multicopter attitude tracking on SO(3). In *IEEE conference on control applications (CCA)*, pages 1160–1166. IEEE, 2015.
- [14] H. Khalil. *Nonlinear Systems*. Prentice Hall, Upper Saddle River, New Jersey, 3rd edition, 2002.
- [15] J. S. Kim, T. W. Yoon, A. Jadbabaie, and C. De Persis. Input-to-state stable finite horizon mpc for neutrally stable linear discrete-time systems with input constraints. *Systems & Control Letters*, 55(4):293–303, 2006.
- [16] A. L’afflitto, R. B. Anderson, and K. Mohammadi. An introduction to nonlinear robust control for unmanned quadrotor aircraft: How to design control algorithms for quadrotors using sliding mode control and adaptive control techniques. *IEEE Control Systems Magazine*, pages 102–121, 2018.
- [17] E. Lefeber, S. J. A. M. Van den Eijnden, and H. Nijmeijer. Almost global tracking control of a quadrotor UAV on SE(3). In *IEEE 56th Annual Conference on Decision and Control (CDC)*, pages 1175–1180, 2017.
- [18] J. Linchant, J. Lisein, J. Semeki, P. Lejeune, and C. Vermeulen. Are unmanned aircraft systems (UASs) the future of wildlife monitoring? a review of accomplishments and challenges. *Mammal Review*, pages 239–252, 2015.
- [19] M. W. Mueller and R. D’Andrea. A model predictive controller for quadcopter state interception. In *European Control Conference (ECC)*, pages 1383–1389, 2013.
- [20] O. J. Rojas and G. C. Goodwin. A simple anti-windup strategy for state constrained linear control. *IFAC Proceedings Volumes*, 35(1):109–114, 2002.
- [21] A. Romero, R. Penicka, and D. Scaramuzza. Time-optimal online replanning for agile quadrotor flight. *IEEE Robotics and Automation Letters*, pages 7730–7737, 2022.
- [22] P. Rudol and P. Doherty. Human body detection and geolocalization for uav search and rescue missions using color and thermal imagery. In *IEEE aerospace conference*, pages 1–8, 2008.
- [23] J. M. Turner. *The economic potential of unmanned aircraft in agricultural and rural electric cooperatives*. PhD thesis, Oklahoma State University, 2016.